Quantum Tunneling in Testosterone 6β-Hydroxylation by Cytochrome P450: Reaction Dynamics Calculations Employing Multiconfiguration Molecular−Mechanical Potential Energy Surfaces†

Yan Zhang and Hai Lin*

Chemistry Department, University of Colorado Denver, Denver, Colorado 80217-3364

Received: February 27, 2009; Revised Manuscript Received: May 7, 2009

Testosterone hydroxylation is a prototypical reaction of human cytochrome P450 3A4, which metabolizes about 50% of oral drugs on the market. Reaction dynamics calculations were carried out for the testosterone 6β-hydrogen abstraction and the 6β-d_1-testosterone 6β-duterium abstraction employing a model that consists of the substrate and the active oxidant compound I. The calculations were performed at the level of canonical variational transition state theory with multidimensional tunneling and were based on a semiglobal full-dimensional potential energy surface generated by the multiconfiguration molecular mechanics technique. The tunneling coefficients were found to be around 3, indicating substantial contributions by quantum tunneling. However, the tunneling made only modest contributions to the kinetic isotope effects. The kinetic isotope effects were computed to be about 2 in the doublet spin state and about 5 in the quartet spin state.

1. Introduction

Testosterone hydroxylation is a prototypical reaction of cytochrome P450 3A4,[1,2] the major human P450 that has a wide range of substrate specificity and metabolizes nearly 50% of the drugs used today.[3] According to the consensus abstraction−rebound mechanism[4] (Scheme 1), the testosterone hydroxylation is initiated by hydrogen abstraction by the active oxidant, the iron−oxo porphyrin π-cation species named compound I (Cpd I). The abstraction is then followed by radical addition of testosterone (the bound step) to yield an alcohol−ferric product complex.[5] Experiments revealed that testosterone hydroxylation takes place almost exclusively on the β face of testosterone, leading to four major products: 6β-, 2β-, 1β-, and 15β-hydroxytestosterone.[6,7] Of special interest is the most prominent reaction pathway, 6β-hydroxylation (Scheme 2), for which the intrinsic kinetic deuterium isotope effects have been measured for the hydrogen abstraction step in the carefully designed experiments by Krauser and Guengerich.[8] On the basis of the very large value (∼15) for the intrinsic kinetic deuterium isotope effects, Krauser and Guengerich argued that the quantum mechanical tunneling was significant during the hydrogen abstraction step of the reaction pathway.[8]

Theoretical studies have contributed to the understanding of C−H hydroxylation by P450 enzymes.[9−20] Recently, we[20] have performed density functional theory model calculations to investigate the testosterone hydroxylation by P450 3A4. Focusing on the H-abstraction step, that is, the step converting species **1** to **2** in Scheme 2, we identified the transition structures for the reactions at the 6β, 2β, 1β, and 15β positions in both the doublet and quartet spin states. The barrier heights were similar in both spin states (generally within ∼1 kcal/mol) and increased in the order of $6\beta \ll 2\beta < 15\beta < 1\beta$ positions. This suggested the regioselectivity preference of $6\beta \gg 2\beta > 15\beta > 1\beta$, which is in good agreement with the experimental findings.[6,7] We also predicted the Wigner tunneling[21] coefficient (κ_W) and the Skodje−Truhlar[22] tunneling coefficients (κ_{STR}) on the basis of the computed barrier heights and the imaginary frequency of vibrational normal mode at the saddle point ($\nu^{\ddagger}$). The calculated κ_W was between 2.5 and 3.5, which seemed "normal"; however, the fact that $|\nu^{\ddagger}| \gg k_B T \approx 200$ cm^{-1} at $T = 300$ K indicated that the calculations of κ_W did not converge. The divergence-free STR model approximates the barrier by an inversed parabola in that it is similar to the Wigner tunneling treatment; but the STR method has a wider range of validity.[22,23] The

SCHEME 1: Model of the Abstraction−Rebound Mechanism

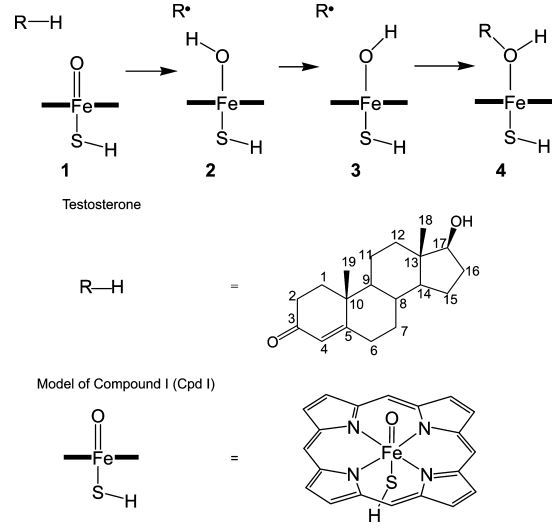

SCHEME 2: Testosterone 6β-Hydroxylation

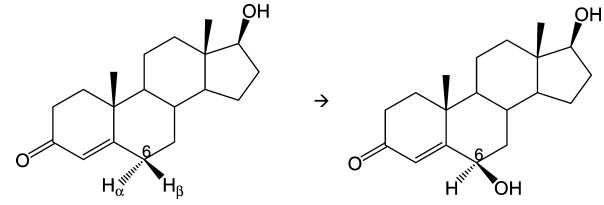

† Part of the "Walter Thiel Festschrift".

* Corresponding author. E-mail: hai.lin@ucdenver.edu.

10.1021/jp901850c CCC: $40.75
Published on Web 05/29/2009

calculated values of κ_{STR} spread in a wide range of 9−1264 and to be appeared unreasonably large for most of the reactions. The significant variations in κ_{STR} also shed doubt on the reliability of the tunneling treatment for those reactions. Clearly, for our system, those two oversimplified tunneling models were not reliable in quantitative prediction for the tunneling coefficients.

The situation invites more advanced reaction dynamics theory into play. One common drawback in the two tunneling models above is that they did not account for the reaction curvature,[24,25] that is, the coupling between the reaction coordinate motion and the vibrations transverse to it. Multidimensional tunneling treatments such as small-curvature tunneling (SCT)[23,24] and large-curvature tunneling (LCT)[24,26,27] treatments take into consideration those couplings and are capable of obtaining more reliable results. The SCT treatment is most accurate when the reaction curvature is small to moderate and the tunneling is confined in the narrow valley centered along the minimum energy path (MEP) that connects the reactants and products.[24] The LCT treatment deals with extensive nonclassical straight-line corner cutting the wider region on the concave side of the MEP.[24] The valley along the MEP and the concave side region together is called the reaction swath.[24]

The SCT and LCT schemes are often applied in conjunction with the variational transition state theory (VTST).[24,25] In the transition state theory (TST), the dynamical bottleneck is assumed to be the saddle point along the reaction path. In contrast, the dynamical bottleneck in VTST is a hypersurface separating the reactant and the product in the multidimensional hyperspace; the dividing hypersurface is called the generalized (variational) transition state, whose location is optimized by the minimization of the rate constants.[24] The combination of VTST with the SCT and LCT schemes has been established and successfully applied to many reactions.[25] It is desirable to apply the VTST/MT (MT = SCT or LCT) treatment to the study of testosterone hydroxylation by P450 3A4.

A high-quality potential energy surface that covers the reaction swath is essential to the reaction dynamics calculations. Ideally, one would perform direct dynamics[28] calculations where the electron-structure potential energy surface is computed on the fly. However, given the large size of the active site of the P450 3A4 and the substrate testosterone, direct dynamics calculations are too expensive to be practical. An alternative option is to use an analytic potential energy surface fitted to electronic-structure energies at selected geometries. To construct such an analytic surface is, however, very challenging: as the number of atoms increases, the dimensionality of the hyperspace grows, and the number of grid points needed as input climbs exponentially, quickly reaching a stage such that this option is no longer feasible if a full-dimensional surface is required.

A promising solution to overcome this difficulty is the so-called multiconfiguration molecular mechanics (MCMM)[29−37] technique, which allows the construction of a semiglobal full-dimensional surface for reaction dynamics calculations with minimum effort. The basic idea[29] of MCMM is to form an electronically diabatic Hamiltonian matrix whose diagonal elements are given by classical molecular mechanics and whose off-diagonal elements are obtained by the (modified) Shepard interpolation of quadratic expansions around a set of points where the electronic-structure data are available. The Born−Oppenheimer potential energy surface is obtained as the lowest eigenvalue of the matrix, and it reproduces the electronic-structure data (energy, gradient, and Hessian) in the vicinity of each input data point.

We should point out that such an idea of nondiagonal representation of the Hamiltonian is not new,[38] and it has been used in a variety of contexts for modeling reactive systems.[39−47] However, the MCMM method has two unique features: (1) MCMM interpolates the off-diagonal elements (resonance integral), which is rather smooth, instead of the potential energy surface, which can take very difficult shapes for modeling. (2) The Shepard interpolation of quadratic expansions in MCMM takes very general form, which employs energy, gradient, and Hessian from electronic-structure calculations. Experimental thermodynamics and kinetics data are often very limited, whereas electronic-structure calculations can be, in principle, carried out for any desired geometries. Therefore, the use of electronic-structure data instead of experimental data allows systematic refinement of the surface by the inclusion of more data points in the interpolation. Moreover, in comparison with the interpolation schemes employing only the energy, the use of the gradient and Hessian information in MCMM interpolation significantly reduces the number of data points needed for the convergence of the reaction dynamics calculations. (In a sense, the use of the energy-only data points is equivalent to implicitly computing the numerical Hessian.) Previous MCMM studies[29−36] have demonstrated that reasonably accurate reaction rates can be obtained by employing very sparse (∼10) input data points for a variety of reactions.

The present study aims to gain deeper insight into the quantum tunneling in the testosterone hydroxylation by P450 3A4. We carried out reaction dynamics calculations at the VTST/MT level employing a semiglobal full-dimensional MCMM surface. To our knowledge, this is the first time that VTST/MT calculations are applied to investigate hydroxylation reactions catalyzed by P450 enzymes. As demonstration, we focused on the 6β H-abstraction, the most prominent reaction for testosterone hydroxylation by P450 3A4, for which the deuterium kinetic isotope effects have been measured.[8]

2. Computation

As in our previous work,[20] Cpd I was modeled as an iron−oxo−porphyrin complex without side chains (Scheme 2). The proximal cysteinate ligand was truncated to HS^-, as suggested by Ogliaro et al.[48] In the present study, all quantum mechanical (QM) calculations were done at the level of density function theory employing the B3LYP[49−51] model using the program Gaussian03.[52] The effective core potential with the double-ζ basis set[53] was selected for iron and the 6-31G[54,55] basis set for the other atoms. In the previous study,[20] we found that the use of the above theory and basis sets gave reasonable energy profiles, which is in good agreement with more elaborate calculations employing larger basis sets. In view of the high computational cost involved in the present study, we felt that this selection of QM theory and basis sets was a reasonable compromise between accuracy and affordability.

We calculated the reaction rates by using the locally modified versions of the MC-TINKERATE2007,[56] MC-TINKER2007,[57] and POLYRATE 9.1[58] programs. We had changed the codes such that calculations for large-size systems (∼100 atoms) are possible. The calculations for the four reactions are denoted as follows: testosterone 6β H-abstraction in the doublet spin state as (H; ^{2}A) and in the quartet spin state as (H; ^{4}A) and 6β-d_1-testosterone 6β D-abstraction in the doublet spin state as (D; ^{2}A) and in the quartet spin state as (D; ^{4}A).

The saddle points of the 6β H-abstractions have been optimized in ref 20 for both the doublet spin state (denoted ^{2}A) and the quartet spin state (denoted ^{4}A). It should be noted that

although the saddle points have the same geometries for the testosterone H-abstraction and for the 6β-d_1-testosterone D-abstraction in a given spin state the MEPs are different in the mass-scaled coordinates. That is, the reaction dynamics calculations actually employed different MEPs for the H- and D-abstractions.

For each reaction, we constructed the MCMM surface by using the reactant complex, product complex, the saddle point (P0), and 17 supplementary Shepard points (P1−P17). The procedure was outlined in Section III of the Supporting Information and is similar to the one recommended in ref 30. The reactant and product complexes were optimized at the MM level, which will explicitly be referred to as MM reactant complex and MM product complex, respectively. The saddle point and all supplementary Shepard points were computed at the QM level of theory. Initially, the surface was constructed without the supplementary points, and the surface is denoted MCMM-0. On the basis of the MCMM-0 surface, the reaction dynamics calculation was performed, which is referred to the MCMM-0 dynamics calculation. Next, the supplementary Shepard points were added successively, one or a few at a time, to refine the MCMM surface. The surface generated by using P1−Pα (α = 1, 2,..., 17) supplementary Shepard points is denoted MCMM-α, and the rate calculations based on the surface is referred to as the MCMM-α dynamics calculation. Among the 17 supplementary Shepard points, P1−P8 were used to follow the MEP, P9−P14 were used to smooth the vibrational adiabatic ground-state potential energy (V_a^G) profile, and P15−P17 were used to explore the surface at the concave side that is critical for LCT calculations. The SCT calculations converged with the inclusion of P1−P14, and they were affected negligibly by P15−P17. The geometries, energies, and frequencies are listed for all supplementary Shepard points in Section III in the Supporting Information.

The MM3[59−61] force field implemented in TINKER[62] was used. Missing parameters were added, which were set to those of the similar atom types or derived from QM calculations.[29,30,33] The added parameters were documented in Section I of the Supporting Information.

The Page−McIver method[63] was chosen to follow the MEP. We have tested different step sizes in the MEP following and found that a step size of 0.005 bohr could produce an accurate MEP. However, to obtain an accurate V_a^G (and the rates), an even smaller step size (0.001 bohr) was recommended. (See also Figures S1 and S2 and Table S1 in the Supporting Information.) To reduce computational effort, we therefore selected the step size of 0.005 bohr in the MCMM-0, MCMM-1,..., MCMM-9 calculations, where the goal was to explore the MEP, and we used 0.001 bohr in the MCMM-10, MCMM-14, and MCMM-17 calculations, where the rates were computed.

The MEP range (in bohr) was $-2.00 \le s \le 0.55$, where s is the signed distance from the saddle point along the mass-scaled reaction coordinate. The coordinates were scaled to a reduced mass, μ, of 1 amu, and a negative value of s indicated a point along the MEP at the reactant side. When it followed the MEP, the Hessian was computed every 10 gradient steps, that is, by a step size of 0.05 bohr in the MCMM-0 to MCMM-9 calculations and 0.01 bohr in the MCMM-10, MCMM-14, and MCMM-17 calculations.

The harmonic approximation was assumed in all cases, and the vibrational analyses were carried out using the redundant internal coordinates listed in Section IV in the Supporting Information. When computing the partition functions, we had adopted a cutoff frequency of 50 cm^{-1}.[64] That is, for a vibrational mode of lower than 50 cm^{-1} frequency, the partition function was evaluated by using 50 cm^{-1} for the frequency. As previously discussed,[64] this is an empirical treatment to avoid the unrealistic estimation of partition functions by the harmonic approximation for vibrations of very low frequencies for which the harmonic approximation is likely a poor one.

Both the TST[24] calculations and canonical variational transition state theory (CVTST or CVT)[24] calculations were carried out. The TST rate was given by

$$k^{TST} = \frac{\sigma}{k_B T}\frac{Q^{\ddagger}}{Q^R}\exp(-V^{\ddagger}/k_B T) \quad (1)$$

where σ is the symmetry factor, k_B is the Boltzmann constant, T is the temperature, $Q^{\ddagger}$ is the partition function for the transition state at the saddle point, Q^R is the partition function for the reactant, and $V^{\ddagger}$ is the barrier height for the reaction. The partition function is the product of the electronic, vibrational, rotational, and translational partition functions

$$Q = Q_{elect}Q_{trans}Q_{vib}Q_{rot} \quad (2)$$

where $Q_{elect} = 1$ in the present study. The CVT rate was computed by

$$k^{CVT} = \frac{\sigma}{k_B T}\frac{Q^{CVT}}{Q^R}\exp(-V_{MEP}(s^*)/k_B T) \quad (3)$$

where Q^{CVT} is the partition function for the variational transition state, s^* is the location of the variational transition state at the MEP in the mass-scaled coordinates, and $V_{MEP}(s^*)$ is the corresponding energy value of the MEP.

We computed the tunneling contributions by employing four different schemes: the Wigner tunneling (W), the zero-curvature tunneling (ZCT), SCT, and LCT. In the ZCT treatment, the reaction curvature is assumed to be zero, and the tunneling path is along the MEP. The ZCT model is less accurate than the SCT and LCT models; nevertheless, we presented the ZCT calculations for reference purpose. The TST rate, k_{TST}, was multiplied by the Wigner tunneling coefficient, κ^W, to yield the Wigner-corrected TST rate, which will be denoted TST/W

$$k^{TST/W} = \kappa^W k^{TST} \quad (4)$$

The CVT rate was multiplied by the tunneling coefficient of ZCT κ^{ZCT} to give the ZCT-corrected CVT rate

$$k^{CVT/ZCT} = \kappa^{ZCT} k^{CVT} \quad (5)$$

which will be denoted CVT/ZCT. The SCT- and LCT-corrected CVT rates are defined in the same way as the ZCT-corrected CVT rate, and they will be denoted CVT/SCT and CVT/LCT, respectively. In the LCT calculations, we had allowed only the tunneling into the ground state of the product to reduce the computational effort. Our previous MCMM dynamics calculations[30,31,33] have showed that the errors incurred by ignoring the tunneling into excited states are usually rather small (typically less than 10%). For the present study, this error is likely to be smaller than the errors due to other sources (e.g., inaccurate barrier heights).

TABLE 1: Electronic-Structure Energetics and Bottleneck Properties at $T = 300$ K for Testosterone 6β H-Abstraction and 6β-d_1-Testosterone 6β D-Abstraction by Compound I by the MCMM-17 Reaction Dynamics Calculations[a]

	(H; ^2A)	(H; ^4A)	(D; ^2A)	(D; ^4A)
$V^{\ddagger}$	9.1	8.7	9.1	8.7
V^{P}	−9.8	−9.5	−9.8	−9.5
$v^{\ddagger}$	1616.0i	1665.0i	1226.3i	1260.5i
V_a^{RG}	459.3	459.5	457.2	457.4
V_a^{PG}	448.4	448.8	446.6	447.0
$V_a^{\ddagger G}$	464.7	464.7	463.7	463.7
s^*	−0.403	−0.044	−0.160	−0.153
$V_a^{G}(s^*)$	465.7	465.1	464.0	463.9
$\Delta V_a^{G}(s^*)$	6.4	5.6	6.8	6.5
$V_{MEP}(s^*)$	6.8	8.7	8.7	8.3
E_{rep}				
ZCT	465.1	464.8	463.5	463.2
SCT	465.0	464.6	463.4	463.2
LCT	464.8	464.4	463.6	463.3

[a] The zero of energy for each reaction is set to the classical potential energy at reactants ($V^R \equiv 0$). $V^{\ddagger}$ is the potential energy at the saddle point (equal to the classical forward barrier height). V^P is the potential energy at the products (equal to the classical energy of reaction). $v^{\ddagger}$ is the imaginary frequency of the vibrational normal mode at the saddle point. V_a^{RG} is the vibrationally adiabatic ground-state potential energy curve at reactants, and the value of this curve is V_a^{PG} at products and $V_a^{\ddagger G}$ at the saddle point. s^* is the location of the variational transition state (dynamical bottleneck) at the minimum energy path in the mass-scaled coordinates. $V_{MEP}(s^*)$ and $V_a^{G}(s^*)$ are the corresponding energy values of the minimum energy path and the adiabatic ground-state potential, respectively, and $\Delta V_a^{G}(s^*) = V_a^{G}(s^*) - V_a^{RG}$. The representative tunneling energies are given as E_{rep} for zero-curvature tunneling (ZCT), small-curvature tunneling (SCT), and large-curvature tunneling (LCT). All energies are in kilocalories per mole, frequencies are in inverse centimeters, and s^* values are in bohr.

3. Results

Table 1 tabulates the electronic-structure energetics as well as the dynamical bottleneck properties at $T = 300$ K. The reactions are exothermic by about 9 kcal/mol. The barrier heights are very similar in both the doublet and quartet spin states, with the quartet spin states having slightly lower (0.4 kcal/mol) barrier heights. The adiabatic ground-state potential energies are also very similar in both spin states for the H-abstractions (and for the D-abstractions). All locations of the dynamical bottleneck are at the reactant side and are close to the saddle point. The result indicates that the free energy barriers are lower for the quartet spin state than for the doublet spin state by about 0.8 kcal/mol for the H-abstraction and by 0.3 kcal/mol for the D-abstraction.

Figure 1 illustrates the MEP curves for all four reactions. For each reaction, we show both the MCMM-10 and MCMM-17 data. We noticed a quick drop of V_{MEP} near $s = 0.5$ bohr in the (H; ^{2}A) reaction. We found that adding more Shepard points did not change much of the shape of the curve; meanwhile, the rate calculations depended negligibly on the MEP of $s > 0.5$ bohr. Figure 2 gives the V_a^G curves for the reactions. Noises (oscillations) have shown up in the V_a^G curve, which is not uncommon for MCMM reaction dynamics calculations; the noises were due to the oscillations in the generalized vibrational frequencies along the MEP. In particular, one can see two sharp peaks in the MCMM-10 V_a^G curves for the (H; ^{2}A) and (D; ^{4}A) reactions. Adding four more Shepard points in each case had removed those peaks and led to much smoother V_a^G. For each reaction, the MCMM-14 V_a^G curve (not shown) differed negligibly from

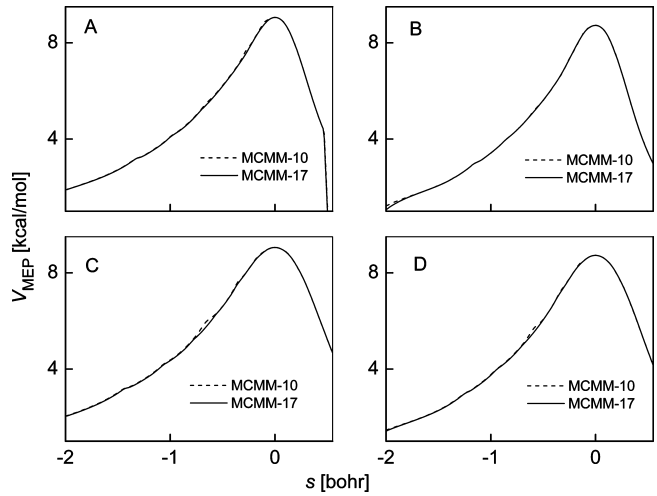

Figure 1. Minimum energy path V_{MEP} as a function of mass-scaled reactant coordinate s by the MCMM-10 and MCMM-17 reaction dynamics calculations for the 6β H-abstraction of testosterone in the (A) doublet and (B) quartet spin states and for the 6β D-abstraction of 6β-d_1-testosterone in the (C) doublet and (D) quartet spin states.

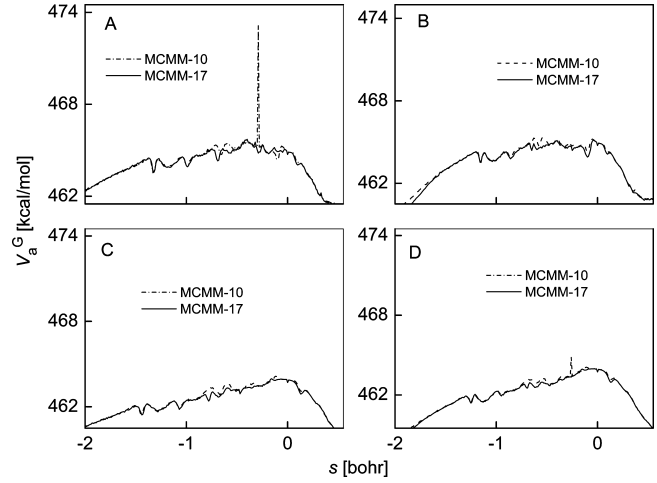

Figure 2. Ground-state adiabatic energy V_a^G at $T = 300$ K as a function of mass-scaled reactant coordinate, s, by the MCMM-10 and MCMM-17 reaction dynamics calculations for the 6β H-abstraction of testosterone in the (A) doublet and (B) quartet spin states and for the 6β D-abstraction of 6β-d_1-testosterone in the (C) doublet and (D) quartet spin states.

the MCMM-17 curve shown in Figure 2. In principle, one can keep adding more points to refine the V_a^G curve; however, that will significantly increase the computational cost and is not necessary if the rate calculations have reasonably converged.

The computed rates and kinetic isotopic effects (k_H/k_D) are listed in Table 2, and the transmission coefficients are provided in Table 3. It is very encouraging to see that the SCT and LCT calculations have indicated rather similar tunneling contributions, suggesting the reliability of the multidimensional tunneling treatments. The Wigner tunneling estimation yields transmission coefficients (2.4 to 3.7) similar to those of the more advanced SCT and LCT treatments for tunneling contributions (2.4 to 3.6). This is, however, just fortunate because the Wigner tunneling calculations did not converge for these reactions. The kinetic isotope effects were predicted to be about 9 by the TST/W calculations for both spin states but were predicted by CVT/SCT (and CVT/LCT) to be about 2 and 5 in the doublet and

TABLE 2: Rate Constant (cm^3 $molecule^{-1}$ s^{-1}) and Kinetic Isotope Effect at $T = 300$ K by the MCMM-17 Reaction Dynamics Calculations[a]

	TST[b]	TST/W[c]	CVT[d]	CVT/ZCT[e]	CVT/SCT[f]	CVT/LCG[g]
^2A						
k^H	4.80×10^{-21}	1.68×10^{-20}	9.57×10^{-24}	2.17×10^{-23}	3.25×10^{-23}	3.18×10^{-23}
k^D	7.50×10^{-22}	1.83×10^{-21}	6.05×10^{-24}	1.14×10^{-23}	1.56×10^{-23}	1.45×10^{-23}
k^H/k^D	6.4	9.2	1.6	1.9	2.1	2.2
^4A						
k^H	3.84×10^{-20}	1.41×10^{-19}	1.48×10^{-22}	2.40×10^{-22}	3.94×10^{-22}	3.49×10^{-22}
k^D	5.81×10^{-21}	1.46×10^{-20}	2.78×10^{-23}	5.93×10^{-23}	8.33×10^{-23}	7.73×10^{-23}
k^H/k^D	6.6	9.6	5.3	4.0	4.7	4.5

[a] Doublet spin state is denoted ^2A, and the quartet spin state is denoted ^4A. k_H is for testosterone 6β H-abstraction, and k_D is for 6β-d_1-testosterone 6β D-abstraction. [b] Transition state theory. [c] Transition state theory with Wigner tunneling. [d] Canonical variational transition state theory. [e] Canonical variational transition state theory with zero-curvature tunneling. [f] Canonical variational transition state theory with small-curvature tunneling. [g] Canonical variational transition state theory with large-curvature tunneling.

TABLE 3: Transmission Coefficients at $T = 300$ K by the MCMM-17 Reaction Dynamics Calculations[a]

	κ_W	κ_{ZCT}	κ_{SCT}	κ_{LCT}
(H; ^2A)	3.5	2.3	3.4	3.3
(H; ^4A)	3.7	1.6	2.7	2.4
(D; ^2A)	2.4	1.9	2.6	2.4
(D; ^4A)	2.5	2.3	3.2	2.9

[a] Testosterone 6β H-abstraction is denoted (H; ^2A) in the doublet spin state and (H; ^4A) in the quartet spin state. The 6β-d_1 -testosterone 6β D-abstraction is denoted (D; ^2A) in the doublet spin state and (D; ^4A) in the quartet spin state. The subscript W labels Wigner tunneling, ZCT labels zero-curvature tunneling, SCT labels small-curvature tunneling, and LCT labels large-curvature tunneling.

quartet spin states, respectively. Interestingly, recent theoretical studies on the *N*,*N*-dimethylaniline hydroxylation[65,66] and on the hydroxylation step in the *N*-dealkylation of *N*-cyclopropyl-*N*-methylaniline,[67] where the Wigner tunneling treatment was adopted, also indicated larger kinetic isotope effects in the high spin state. After taking into account the tunneling contributions, we found that the rates are faster in the quartet spin state than in the doublet spin state by a factor of about 10 for the H-abstraction and by a factor of about 5−8 for the D-abstraction. Therefore, our calculations suggested that the reactions in the quartet spin state dominated and that the overall kinetic isotope effect is about 5.

4. Discussion

The multidimensional tunneling (SCT and LCT) coefficients in Table 3 indicated the substantial involvement of tunneling in the reactions at $T = 300$ K, which is in agreement with the experimental implication.[8] The transmission coefficients were computed to be larger in the doublet spin state (~3.3) than in the quartet spin state (~2.5) for the H-abstractions. For the D-abstractions, the tunneling contribution was, however, predicted to be more prominent in the quartet spin state (~3.0) than in the doublet spin state (~2.5). For comparison, the Wigner tunneling calculations essentially yielded the same tunneling coefficients in both spin states, owing to the very similar imaginary frequencies at the saddle points in (H; ^{2}A) and (H; ^{4}A) as well as in (D; ^{2}A) and (D; ^{4}A). (See Table 1.) The difference between κ_W and κ_{MT} (MT = SCT and LCT) reflects the dependence of multidimensional tunneling models on the reaction curvature and on the potential energy surface in the reaction swath, which are either ignored or greatly simplified in the Wigner tunneling model.

How did the multidimensional tunneling contribution affect the kinetic isotope effects, in comparison with other contributions? To answer this question, we have made a detailed factor analysis for the kinetic isotope effects in Table 4, where

TABLE 4: Factors for Kinetic Isotope Effects[a]

	η_{trans}	η_{rot}	η_{vib}	η_{pot}	η_{tunnel} SCT	η_{tunnel} LCT
^2A	1.00	1.01	0.07	24.43	1.32	1.39
^4A	1.00	1.01	9.23	0.56	0.85	0.81

[a] See eqs 7−10 and the text for the definitions.

$$k_H/k_D = \eta_{total} \tag{6}$$

$$\eta_{total} = \eta_{trans}\eta_{rot}\eta_{vib}\eta_{pot}\eta_{tunnel} \tag{7}$$

Here η_{trans}, η_{rot}, and η_{vib} are the factor contributions to the kinetic isotope effects by the translational, rotational, and vibrational partition functions, respectively, η_{pot} is by the potential energy at the dynamical bottleneck, and η_{tunnel} is by the quantum tunneling. The calculations for η_{trans} were as follows

$$\eta_{trans} = \frac{Q^{CVT}_{trans}(H)/Q^{R}_{trans}(H)}{Q^{CVT}_{trans}(D)/Q^{R}_{trans}(D)} \tag{8}$$

where Q^{CVT}_{trans} is the translational partition function at the generalized transition state and Q^{R}_{trans} is the translational partition function at the reactants. η_{rot} and η_{vib} were evaluated in a similar way. The η_{pot} was computed by

$$\eta_{pot} = \frac{\exp(-V^{H}_{MEP}(s^*))}{\exp(-V^{D}_{MEP}(s^*))} \tag{9}$$

where $V^{H}_{MEP}(s^*)$ and $V^{D}_{MEP}(s^*)$ are the MEP energies at the generalized transition states for H and D reactions, respectively; they were the same in TST but different in CVT. The η_{tunnel} was given by

$$\eta_{tunnel} = \kappa^{MT}_{H}/\kappa^{MT}_{D} \tag{10}$$

where MT = SCT or LCT.

As expected, the translational and rotational partition functions had few contributions to the kinetic isotope effects because the

change in the mass is very small for such a large system. In contrast, the vibrations played a critical role because both the η_{vib} and η_{pot} significantly deviated from 1. We note that η_{vib} and the η_{pot} tend to cancel each other because a given vibrational mode has opposite tendencies in making its contributions to the vibrational partition function and to the V_a^G. For example, a low-frequency mode brings a large value to the vibrational partition function but adds little to the V_a^G. (Note that the dynamical bottleneck and therefore the $V_{MEP}(s^*)$ are determined through the V_a^G.) It would be more instructive to combine the η_{vib} and the η_{pot} together, and multiplying those two gives 1.6 for the doublet spin state and 5.1 for the quartet spin state. The quantum tunneling, although involved substantially in the reactions, brought only modest changes to the kinetic isotope effects.

The multidimensional tunneling calculations predicted that quantum tunneling enlarged the kinetic isotope effects in the doublet spin state (by a factor of 1.3 to 1.4) but reduced them in the quartet spin state (by a factor of about 0.8); such a finding is somewhat surprising. A possible explanation is a narrower barrier for D tunneling than for H tunneling in the quartet spin state. (Recall that the MEP for H and for D abstractions was different in the mass-scaled coordinate system.) The similar κ_{SCT} and κ_{LCT} values for a given H (D) abstraction supported this claim because the SCT and LCT tunneling paths were completely different. Another possibility is that the constructed MCMM surfaces were not accurate enough, which may be due to the following reasons.

First, it could be that the electronic-structure information used for the construction of the potential energy surfaces is not accurate enough. The MCMM surface was based on electronic-structure data points calculated by employing the theory and basis sets specified in Section II. Although they help to reduce the computational cost, the selected theory and basis sets might not be sufficient in providing the needed accuracy for the energetics (energies, gradients, and Hessians). As the second derivative of energy, Hessian is particularly difficult to obtain with high accuracy. However, Hessian plays a critical role in the Shepard interpolation in the multidimensional hyperspace. Inaccurate Hessians might have led to the errors in the calculations of the generalized vibrational normal modes along the MEP and in turn to the errors in the free energy profile on which the generalized transition state was located and the tunneling calculations were carried out.

Second, errors in the MCMM surfaces might also be incurred because of the use of sparse Shepard points for interpolation in the multidimensional hyperspace. With only eight data points as input, the MEP had been well converged. However, obtaining a smooth V_a^G was far more challenging, and we could still see the noises in the MCMM-17 V_a^G curves. Using more data points could help to make them smoother, but that would greatly increase the computational cost in the electronic-structure calculations (dominated by Hessian calculations), which was not practical given the large size of the system in question. Moreover, the time required for MCMM calculations also significantly increased as more data points were used as input, making it more and more difficult to add data points in the successive "prediction-correction" manner. (Currently, the MCMM-17 reaction dynamics calculations for one reaction will take about 50 h on an IBM power4 CPU.) In the future, it will be helpful to parallelize the codes and to improve the efficiency in handling the huge-size Hessians. The noises in the V_a^G curve might lead to the errors in locating the dynamic bottleneck; fortunately, their effects to tunneling calculations were much smaller because the integration effectively averaged and thus greatly reduced the noises.[31] It would be helpful to optimize the weight function[29] used in the modified Shepard interpolation (which is certainly not trivial) to minimize the noises in the V_a^G curve.

Reaction dynamics simulations for large systems are very challenging, especially when the goal is to obtain data accurate enough that it can be compared with experiments. The computed kinetic isotope effects (~5) in this work are smaller than the one (~15) established by the experiments.[8] The discrepancies may due to several reasons. The first possibility is the limited accuracy for the potential energy surface, which has just been discussed above. Another possible reason is the use of the cutoff frequency in the evaluation of the vibrational partition functions. The vibrational normal-mode analysis at the stationary geometries and the generalized vibrational normal-mode analysis along the MEP had yielded many low frequency (<50 cm^{-1}) modes. This is not surprising given the large size of our model system. Those modes are likely to be extremely unharmonic, and their partition functions might be significantly overestimated if the harmonic approximation is used. However, there was no general and simple way to solve this problem at this moment.[68] Our use of a cutoff frequency of 50 cm^{-1} helped to avoid the unrealistically large values in the partition function calculations, but it eliminates the frequency changes in those modes due to the deuterium substitution, and that might have introduced errors.

Finally, we note that the present calculations are gas-phase model calculations, which did not take into account the complex environment where the reactions actually take place. An early combined quantum-mechanics/molecular-mechanics (QM/MM)[69−74] study on P450cam by Shaik, Thiel, and coworkers[75] has revealed that the oxidant Cpd I behaves as a chameleon species that adapts its electronic and structural character to the specific environment. More recently, a QM/MM study on P450 3A4 showed that the electronic structure of Cpd I depends subtly on the interactions between Cpd I and residues A305, T309, I443, and G444.[76] It is conceivable that the potential surface for testosterone hydroxylation will be finely tuned by the small changes of the architecture of the active site pocket in P450 3A4. VTST/MT calculations that take into consideration the effects due to the protein matrix and solvent are therefore highly desirable.[77,78] To this end, we would combine the QM/MM and MCMM techniques to generate the potential surfaces for reaction dynamics calculations. The research in this direction has received much attention in the past few years.[31,33,36,37] In particular, we point to the recent progress in the electrostatic-embedding MCMM[36,37] methodology. Although test calculations[37] have only been carried out for systems that have small QM subsystems, the method is very promising and might be further developed and coded (e.g., to combine with the appropriate boundary treatments[79−81]) for the study of enzyme reaction dynamics.

5. Conclusions

To summarize, we have presented the VTST/MT reaction dynamics calculations on the testosterone hydroxylation by P450 3A4, which were based on a semiglobal full-dimensional potential energy surface generated by the MCMM technique. These are the first VTST/MT calculations on the hydroxylation reactions catalyzed by P450 enzymes. The tunneling coefficients were found to be around 3, indicating substantial contributions by quantum tunneling. However, tunneling made only modest contributions to the kinetic isotope effects. The kinetic isotope

effects were computed to be about 2 in the low spin state and about 5 in the high spin state, both of which are significantly smaller than the experimental value (15). The discrepancies between the calculations and experiments may due to the limited accuracy in the potential energy surfaces, the approximate treatment in calculating the partition function for low-frequency vibrational modes, or the use of gas-phase model without considering the protein−solvent environment.

Ideally, to investigate the quantum effects in reactions, one would carry out full quantum dynamics calculations, where all degrees of freedom for the nuclei are treated quantum mechanically; but such calculations are too expensive and are nowadays only feasible for systems up to a few (six) atoms.[82] The VTST/MT calculations are more practical for larger reactive systems. This work demonstrates that by employing the MCMM method in the construction of semiglobal potential energy surface, VTST/MT can be applied to systems of about 100 atoms. The application of the MCMM-based VTST/MT calculations to even larger systems can be done when combined with the QM/MM technique.

Acknowledgment. This research is supported by the Research Corporation. We thank the National Cancer Institute−Frederick Advanced Biomedical Computing Center for providing CPU time and access to the *Gaussian03* program.

Supporting Information Available: Added MM3 parameters in the MM3 parameter file (MM3-1996) in the TINKER format for the MCMM calculation; input geometries, absolute energy, and frequencies in the MCMM calculations and of the supplementary Shepard points in the MCCM calculations for 6β-H abstraction of testosterone (and 6β-D abstraction of 6β-d_1-tesosterone) by compound I, atomic index and the internal coordinates used for generalized normal mode analysis in the MCMM reaction dynamics calculations, V_{MEP} as a function of mass-scaled reactant coordinate s, V_a^G at $T = 300$ K as a function of mass-scaled reactant coordinate s, and rate constants and transmission coefficients by MCMM-10 reaction dynamics calculations. This material is available free of charge via the Internet at http://pubs.acs.org.

References and Notes

(1) *Cytochrome P450: Structure, Mechanisms and Biochemistry*, 3rd ed.; Ortiz de Montellano, P. R., Ed.; Kluwer/Plenum: New York, 2005.
(2) Guengerich, F. P. *Annu. Rev. Pharmacol. Toxicol.* **1999**, *39*, 1.
(3) Evans, W. E.; Relling, M. V. *Science* **1999**, *286*, 487.
(4) Groves, J. T.; McClusky, G. A. *J. Am. Chem. Soc.* **1976**, *98*, 859.
(5) Groves, J. T.; Watanabe, Y. *J. Am. Chem. Soc.* **1988**, *110*, 8443.
(6) Waxman, D. J.; Attisano, C.; Guengerich, F. P.; Lapenson, D. P. *Arch. Biochem. Biophys.* **1988**, *263*, 424.
(7) Krauser, J. A.; Voehler, M.; Tseng, L.-H.; Schefer, A. B.; Godejohann, M.; Guengerich, F. P. *Eur. J. Biochem.* **2004**, *271*, 3962.
(8) Krauser, J. A.; Guengerich, F. P. *J. Biol. Chem.* **2005**, *280*, 19496.
(9) Shaik, S.; Kumar, D.; de Visser, S. P.; Altun, A.; Thiel, W. *Chem. Rev.* **2005**, *105*, 2279.
(10) Harris, N.; Cohen, S.; Filatov, M.; Ogliaro, F.; Shaik, S. *Angew. Chem., Int. Ed.* **2000**, *39*, 2003.
(11) Kamachi, T.; Yoshizawa, K. *J. Am. Chem. Soc.* **2003**, *125*, 4652.
(12) Park, J. Y.; Harris, D. *J. Med. Chem.* **2003**, *46*, 1645.
(13) Guallar, V.; Friesner, R. A. *J. Am. Chem. Soc.* **2004**, *126*, 8501.
(14) Schöneboom, J. C.; Cohen, S.; Lin, H.; Shaik, S.; Thiel, W. *J. Am. Chem. Soc.* **2004**, *126*, 4017.
(15) Altun, A.; Guallar, V.; Friesner, R. A.; Shaik, S.; Thiel, W. *J. Am. Chem. Soc.* **2006**, *128*, 3924.
(16) Bach, R. D.; Dmitrenko, O. *J. Am. Chem. Soc.* **2006**, *128*, 1474.
(17) Wang, Y.; Wang, H.; Wang, Y.; Yang, C.; Yang, L.; Han, K. *J. Phys. Chem. B* **2006**, *110*, 6154.
(18) Liu, X.; Wang, Y.; Han, K. *J. Bio. Inorg. Chem.* **2007**, *12*, 1073.
(19) Wang, Y.; Yang, C.; Wang, H.; Han, K.; Shaik, S. *ChemBioChem* **2007**, *8*, 277.
(20) Zhang, Y.; Morisetti, P.; Kim, J.; Smith, L.; Lin, H. *Theor. Chem. Acc.* **2008**, *121*, 313.
(21) Wigner, E. *Z. Physik. Chem. B* **1932**, *19*, 203.
(22) Skodje, R. T.; Truhlar, D. G. *J. Phys. Chem.* **1981**, *85*, 624.
(23) Skodje, R. T.; Truhlar, D. G.; Garrett, B. C. *J. Phys. Chem.* **1981**, *85*, 3019.
(24) Truhlar, D. G.; Isaacson, A. D.; Garrett, B. C. Generalized Transition State Theory. In *Theory of Chemical Reaction Dynamics*; Baer, M., Ed.; CRC Press: Boca Raton, FL, 1985; Vol. 4, p 65.
(25) Truhlar, D. G.; Garrett, B. C.; Klippenstein, S. J. *J. Phys. Chem.* **1996**, *100*, 12771.
(26) Garrett, B. C.; Truhlar, D. G.; Wagner, A. F.; Dunning, T. H., Jr. *J. Chem. Phys.* **1983**, *78*, 4400.
(27) Lu, D.-h.; Truong, T. N.; Melissas, V. S.; Lynch, G. C.; Liu, Y.-P.; Garrett, B. C.; Steckler, R.; Isaacson, A. D.; Rai, S. N.; Hancock, G. C.; Lauderdale, J. G.; Joseph, T.; Truhlar, D. G. *Comput. Phys. Commun.* **1992**, *71*, 235.
(28) Truhlar, D. G.; Gordon, M. S. *Science* **1990**, *249*, 491.
(29) Kim, Y.; Corchado, J. C.; Villa, J.; Xing, J.; Truhlar, D. G. *J. Chem. Phys.* **2000**, *112*, 2718.
(30) Albu, T. V.; Corchado, J. C.; Truhlar, D. G. *J. Phys. Chem. A* **2001**, *105*, 8465.
(31) Lin, H.; Pu, J. Z.; Albu, T. V.; Truhlar, D. G. *J. Phys. Chem. A* **2004**, *108*, 4112.
(32) Kim, K. H.; Kim, Y. *J. Chem. Phys.* **2004**, *120*, 623.
(33) Lin, H.; Zhao, Y.; Tishchenko, O.; Truhlar, D. G. *J. Chem. Theory Comput.* **2006**, *2*, 1237.
(34) Tishchenko, O.; Truhlar, D. G. *J. Phys. Chem. A* **2006**, *110*, 13530.
(35) Tishchenko, O.; Truhlar, D. G. *J. Chem. Theory Comput.* **2007**, *3*, 938.
(36) Higashi, M.; Truhlar, D. G. *J. Chem. Theory Comput.* **2008**, *4*, 790.
(37) Higashi, M.; Truhlar, D. G. *J. Chem. Theory Comput.* **2008**, *4*, 1032.
(38) Truhlar, D. G. *J. Phys. Chem. A* **2002**, *106*, 5048.
(39) London, F. *Z. Elektrochem.* **1929**, *35*, 552.
(40) Eyring, H.; Polanyi, M. *Z. Phys. Chem. B* **1931**, *12*, 279.
(41) Parr, C. A.; Truhlar, D. G. *J. Phys. Chem.* **1971**, *75*, 1844.
(42) Vila, C. L.; Kinsey, J. L.; Ross, J.; Schatz, G. C. *J. Chem. Phys.* **1979**, *70*, 2414.
(43) Warshel, A.; Weiss, R. M. *J. Am. Chem. Soc.* **1980**, *102*, 6218.
(44) Pross, A.; Shaik, S. S. *Acc. Chem. Res.* **1983**, *16*, 363.
(45) Chang, Y. T.; Miller, W. H. *J. Phys. Chem.* **1990**, *94*, 5884.
(46) Mo, Y.; Gao, J. *J. Phys. Chem. A* **2000**, *104*, 3012.
(47) Lefohn, A. E.; Ovchinnikov, M.; Voth, G. A. *J. Phys. Chem. B* **2001**, *105*, 6628.
(48) Ogliaro, F.; Cohen, S.; Filatov, M.; Harris, N.; Shaik, S. *Angew. Chem., Int. Ed.* **2000**, *39*, 3851.
(49) Becke, A. D. *Phys. Rev. A* **1988**, *38*, 3098.
(50) Becke, A. D. *J. Chem. Phys.* **1993**, *98*, 5648.
(51) Lee, C.; Yang, W.; Parr, R. G. *Phys. Rev. B: Condens. Matter Mater. Phys.* **1988**, *37*, 785.
(52) Frisch, M. J.; Trucks, G. W.; Schlegel, H. B.; Scuseria, G. E.; Robb, M. A.; Cheeseman, J. R.; Montgomery, J. A., Jr.; Vreven, T.; Kudin, K. N.; Burant, J. C.; Millam, J. M.; Iyengar, S. S.; Tomasi, J.; Barone, V.; Mennucci, B.; Cossi, M.; Scalmani, G.; Rega, N.; Petersson, G. A.; Nakatsuji, H.; Hada, M.; Ehara, M.; Toyota, K.; Fukuda, R.; Hasegawa, J.; Ishida, M.; Nakajima, T.; Honda, Y.; Kitao, O.; Nakai, H.; Klene, M.; Li, X.; Knox, J. E.; Hratchian, H. P.; Cross, J. B.; Adamo, C.; Jaramillo, J.; Gomperts, R.; Stratmann, R. E.; Yazyev, O.; Austin, A. J.; Cammi, R.; Pomelli, C.; Ochterski, J. W.; Ayala, P. Y.; Morokuma, K.; Voth, G. A.; Salvador, P.; Dannenberg, J. J.; Zakrzewski, V. G.; Dapprich, S.; Daniels, A. D.; Strain, M. C.; Farkas, O.; Malick, D. K.; Rabuck, A. D.; Raghavachari, K.; Foresman, J. B.; Ortiz, J. V.; Cui, Q.; Baboul, A. G.; Clifford, S.; Cioslowski, J.; Stefanov, B. B.; Liu, G.; Liashenko, A.; Piskorz, P.; Komaromi, I.; Martin, R. L.; Fox, D. J.; Keith, T.; Al-Laham, M. A.; Peng, C. Y.; Nanayakkara, A.; Challacombe, M.; Gill, P. M. W.; Johnson, B.; Chen, W.; Wong, M. W.; Gonzalez, C.; Pople, J. A. *Gaussian03*; Gaussian, Inc.: Pittsburgh, PA, 2003.
(53) Hay, P. J.; Wadt, W. R. *J. Chem. Phys.* **1985**, *82*, 299.
(54) Ditchfield, R.; Hehre, W. J.; Pople, J. A. *J. Chem. Phys.* **1971**, *54*, 724.
(55) Hehre, W. J.; Ditchfield, R.; Pople, J. A. *J. Chem. Phys.* **1972**, *56*, 2257.
(56) Albu, T. V.; Tishchenko, O.; Corchado, J. C.; Kim, Y.; Villà, J.; Xing, J.; Lin, H.; Truhlar, D. G. *MC-TINKERATE2007*; University of Minnesota: Minneapolis, 2007.
(57) Tishchenko, O.; Albu, T. V.; Corchado, J. C.; Kim, Y.; Villà, J.; Xing, J.; Lin, H.; Truhlar, D. G. *MC-TINKER2007*; University of Minnesota: Minneapolis, 2007.
(58) Corchado, J. C.; Chuang, Y.-Y.; Fast, P. L.; Villà, J.; Hu, W.-P.; Liu, Y.-P.; Lynch, G. C.; Nguyen, K. A.; Jackels, C. F.; Melissas, V. S.; Lynch, B. J.; Rossi, I.; Coitiño, E. L.; Fernandez-Ramos, A.; Pu, J.; Albu,

T. V.; Steckler, R.; Garrett, B. C.; Isaacson, A. D.; Truhlar, D. G. *POLYRATE*, version 9.1; University of Minnesota: Minneapolis, 2002.

(59) Allinger, N. L.; Yuh, Y. H.; Lii, J. H. *J. Am. Chem. Soc.* **1989**, *111*, 8551.

(60) Lii, J. H.; Allinger, N. L. *J. Am. Chem. Soc.* **1989**, *111*, 8566.

(61) Lii, J. H.; Allinger, N. L. *J. Am. Chem. Soc.* **1989**, *111*, 8576.

(62) Ponder, J. W. *TINKER*, version 3.5; Washington University: St. Louis, MO, 1997.

(63) Page, M.; McIver, J. W., Jr. *J. Chem. Phys.* **1988**, *88*, 922.

(64) Lin, H.; Zhao, Y.; Ellingson, B. A.; Pu, J.; Truhlar, D. G. *J. Am. Chem. Soc.* **2005**, *127*, 2830.

(65) Li, C.; Wu, W.; Kumar, D.; Shaik, S. *J. Am. Chem. Soc.* **2006**, *128*, 394.

(66) Wang, Y.; Kumar, D.; Yang, C.; Han, K.; Shaik, S. *J. Phys. Chem. B* **2007**, *111*, 7700.

(67) Li, D.; Wang, Y.; Yang, C.; Han, K. *Dalton Trans.* **2009**, 291.

(68) Ellingson, B. A.; Pu, J.; Lin, H.; Zhao, Y.; Truhlar, D. G. *J. Phys. Chem. A* **2007**, *111*, 11706.

(69) Warshel, A.; Levitt, M. *J. Mol. Biol.* **1976**, *103*, 227.

(70) Singh, U. C.; Kollman, P. A. *J. Comput. Chem.* **1984**, *5*, 129.

(71) Field, M. J.; Bash, P. A.; Karplus, M. *J. Comput. Chem.* **1990**, *11*, 700.

(72) *Combined Quantum Mechanical and Molecular Mechanical Methods*; Gao, J., Thompson, M. A., Eds.; ACS Symposium Series 712; American Chemical Society: Washington, DC, 1998.

(73) Lin, H.; Truhlar, D. G. *Theor. Chem. Acc.* **2007**, *117*, 185.

(74) Senn, H. M.; Thiel, W. *Top. Curr. Chem.* **2007**, *268*, 173.

(75) Schöneboom, J. C.; Lin, H.; Reuter, N.; Thiel, W.; Cohen, S.; Ogliaro, F.; Shaik, S. *J. Am. Chem. Soc.* **2002**, *124*, 8142.

(76) Fishelovitch, D.; Hazan, C.; Hirao, H.; Wolfson, H. J.; Nussinov, R.; Shaik, S. *J. Phys. Chem. B* **2007**, *111*, 13822.

(77) Truhlar, D. G.; Gao, J.; Alhambra, C.; Garcia-Viloca, M.; Corchado, J.; Sanchez, M. L.; Villa, J. *Acc. Chem. Res.* **2002**, *35*, 341.

(78) Gao, J.; Truhlar, D. G. *Annu. Rev. Phys. Chem.* **2002**, *53*, 467.

(79) Lin, H.; Truhlar, D. G. *J. Phys. Chem. A* **2005**, *109*, 3991.

(80) Zhang, Y.; Lin, H.; Truhlar, D. G. *J. Chem. Theory Comput.* **2007**, *3*, 1378.

(81) Zhang, Y.; Lin, H. *J. Chem. Theory Comput.* **2008**, *4*, 414.

(82) Ju, L.; Han, K.; Zhang, J. Z. H. *J. Comput. Chem.* **2009**, *30*, 305.

JP901850C